

# Improving machine learning-based weather forecast post-processing with clustering and transfer learning

Yuwen Chen<sup>1</sup>, Xiaomeng Huang<sup>1,2,3</sup>, Yi Li<sup>1,3</sup>, Yue Chen<sup>1</sup>, Chi Yan Tsui<sup>3</sup>, Xing  
Huang<sup>1,3</sup>, Mingqing Wang<sup>1,3</sup>, Jonathon S. Wright<sup>1</sup>

<sup>1</sup>Ministry of Education Key Laboratory for Earth System Modeling, Department of Earth System  
Science, Tsinghua University, Beijing 100084, China

<sup>2</sup>Laboratory for Regional Oceanography and Numerical Modeling, Qingdao National Laboratory for  
Marine Science and Technology, Qingdao, 266237, China

<sup>3</sup>National Supercomputing Center in Wuxi, Wuxi, 214011, China

## Key Points:

- A post-processing framework comprising clustering, decision tree, and transfer learning methods is employed to improve weather forecasts.
- This framework reduces the root-mean-square error by 27.9% (0.81°C) compared to operational ECMWF forecasts.
- Transfer learning improves forecasts by 36.4% at new stations with only one year of data available, reducing barriers to network expansion.

---

Corresponding author: Xiaomeng Huang, [hxm@tsinghua.edu.cn](mailto:hxm@tsinghua.edu.cn)

## Abstract

Machine learning has been widely applied in numerical weather prediction, but the incorporation of new observational sites into models trained on stations with long historical records remains a challenge. Here we propose a post-processing framework consisting of three machine learning methods: station clustering with  $K$ -means, temperature prediction based on decision trees, and transfer learning for newly-built stations. We apply this framework to post-processing forecasts of surface air temperature at 301 weather stations in China. The results show significant reductions (as much as 39.4%~20.0%) in the root-mean-square error of operational forecasts at lead times as long as 7 days. Moreover, the use of transfer learning to incorporate new stations improves forecasts at the new site by 36.4% after only one year of data collection. These results demonstrate the potential for clustering and transfer learning to boost existing applications of machine learning techniques in weather forecasting.

## Plain Language Summary

Statistical approaches have been used for decades to enhance and interpret numerical weather forecasts. Artificial intelligence models have greatly advanced this field but the extension of these models to newly-built sites remains a challenge. To address this, we design a framework that combines three machine learning methods: clustering to group similar stations, decision trees to classify the forecasts, and transfer learning to adapt the model to new stations. We apply this framework to real forecasts and evaluate it against measurements from hundreds of weather stations in China. Station clustering and transfer learning both substantially improve predictions for recently-built sites, demonstrating how these tools can supplement existing artificial intelligence techniques in weather forecasting.

## 1 Introduction

The skill of numerical weather prediction (NWP) has improved significantly in recent decades due to advances in numerical models, data assimilation, and observation systems (Bauer et al., 2015). Nevertheless, the accuracy of NWP is still limited by imperfect model physics, numerical schemes, and initial/boundary conditions (Bauer et al., 2015; Lynch, 2008). Following the pioneering work of Glahn and Lowry (1972), Model Output Statistics (MOS) have been used operationally for over forty years. Raw model forecasts are post-processed using statistical relationships between observations and NWP results. However, the volume and variety of observational and model output data are increasingly overwhelming conventional implementations of these methods (e.g., Agapiou, 2017; Overpeck et al., 2011).

The emergence of machine learning (ML) techniques has provided new perspectives in this field (e.g., Reichstein et al., 2019). The climate community has increasingly turned to such techniques for applications such as improving subgrid-scale parameterizations in numerical models (e.g., Gentile et al., 2018; Rasp et al., 2018; Schneider et al., 2017; Jiang et al., 2018), improving forecasts at very short or very long lead times (e.g., Shi et al., 2015; Ham et al., 2019; B. Pan et al., 2019), detecting extreme weather (Hwang et al., 2019), and identifying complex teleconnection patterns (e.g., Runge et al., 2019; Boers et al., 2019). ML techniques could also substantially improve the accuracy of NWP results (McGovern et al., 2017; Rasp & Lerch, 2018; Scher, 2018).

The success of ML relies heavily on the quality and quantity of training data. Unfortunately, observations are usually sparse, especially for newly-built weather stations. Essential questions therefore arise regarding whether and by what means models trained on data-rich stations can be reliably extended to newly-built stations with limited data records.

66 Clustering techniques are widely used to extract information hidden in complex spatio-  
 67 temporal data (Bador et al., 2015). Stations classified within the same cluster often share  
 68 similar meteorological features. This type of feature-based classification provides a nat-  
 69 ural foundation for transfer learning, a technique by which knowledge gained in complet-  
 70 ing one task is repurposed for a different but related task (S. J. Pan & Yang, 2010). These  
 71 methods may permit models trained for data-rich stations to be rapidly fine-tuned for  
 72 application to data-poor stations. To take full advantage of these techniques, we pro-  
 73 pose a new framework that combines three different ML methods: Clustering, Decision  
 74 trees, and Transfer learning, or CDT for short. We apply CDT to surface air temper-  
 75 ature forecasts as an illustrative validation of this framework and its applicability.

## 76 2 Data

77 NWP data are provided by The International Grand Global Ensemble (TIGGE)  
 78 project of the European Centre for Medium-Range Weather Forecasts (ECMWF) (e.g.,  
 79 Bougeault et al., 2010; Swinbank et al., 2016). The numerical forecasts are initialized  
 80 twice per day at 00 and 12 UTC with lead times ranging from 6 to 168 hours at 6-hour  
 81 increments (for a total of 28 lead times). We use data for the period from 1 January 2013  
 82 to 31 December 2018. The sample size is therefore 4384 for each weather station and lead  
 83 time. Five variables are selected: temperature and dew point temperature at 2 m height,  
 84 surface pressure, and the zonal and meridional wind components at 10 m height.

85 Observations from weather stations in China are obtained from [www.meteomanz.com](http://www.meteomanz.com)  
 86 for the same period (1 January 2013 through 31 December 2018). As too few data are  
 87 available in Xizang and Qinghai, we omit these areas from the analysis. We select 301  
 88 weather stations with data covering at least half of the year 2018 (the testing period as  
 89 introduced below). Four variables (surface air temperature, surface pressure, surface air  
 90 relative humidity, and near-surface wind speed) are provided every 3 hours (00, 03, 06,  
 91 09, 12, 15, 18, and 21 UTC). Static information for each station is also used, including  
 92 latitude, longitude, and elevation. Missing values are filled via linear interpolation in the  
 93 time dimension.

94 The historical observations are processed to generate feature vectors with shapes  
 95 defined by  $(n_{\text{samples}}, n_{\text{steps}}, n_{\text{features}})$ , where  $n_{\text{samples}}$  is the number of records for a spec-  
 96 ified station,  $n_{\text{steps}}$  is the number of time steps used for temporal pattern mining, and  
 97  $n_{\text{features}}$  is equal to 4 (i.e., the number of measurements to match at each time step). For  
 98 example, the shape of the input vector for the Beijing station is (4384, 25, 4) when three  
 99 days of past observations are used. NWP data are interpolated to each station location  
 100 using an inversion-distance weighting (IDW) (Myers, 1994) applied to forecast data from  
 101 the four nearest model grid cells. The observational and NWP data are combined for  
 102 input to the CDT framework.

## 103 3 Methods

104 The CDT framework consists of three individual ML modules: clustering, decision-  
 105 tree, and transfer learning. The clustering module classifies the 301 stations into groups  
 106 using the traditional  $K$ -means technique. Separate decision-tree-based post-processing  
 107 modules are then developed for each cluster and each lead time. Each newly-built sta-  
 108 tion is assigned to the best-fit existing cluster. The transfer learning module is then used  
 109 to produce the final results.

### 110 3.1 Clustering Stations with $K$ -means

111 The traditional  $K$ -means (Hastie et al., 2009) clustering technique is often used for  
 112 climate data analysis (e.g., Bador et al., 2015; Bernard et al., 2013). Stations with sim-  
 113 ilar features are categorized into  $K$  individual clusters by calculating the feature distance

114 between them. The features used in this study are the annual averages and standard de-  
 115 viations of surface air temperature, surface air relative humidity, near-surface wind speed,  
 116 surface pressure, latitude, longitude, and elevation. Models are established and trained  
 117 for each cluster instead of for each station to reduce the computational cost and enlarge  
 118 the training sample for each model.

119 The clustering result is highly sensitive to the value of  $K$ . We use the Silhouette  
 120 Coefficient (Rousseeuw, 1987) to identify the optimal value of  $K$ . This metric measures  
 121 the consistency of samples within each cluster as the ratio between cluster tightness and  
 122 cluster dissociation. A larger Silhouette Coefficient indicates an increase in the inter-cluster  
 123 distance relative to the intra-cluster distance. The maximum coefficient thus marks the  
 124 optimal clustering result according to this metric.

125 The average Silhouette Coefficient (ASC; Text S1 in the supporting information)  
 126 varies with the number of clusters  $K$  (Fig. 1a). We use the ASC to reduce the number  
 127 of candidate  $K$  values so that we do not need to train ML models for all possible val-  
 128 ues of  $K$ . Although the ASC is useful for identifying potential optimal values of  $K$ , a  
 129 larger ASC does not necessarily translate to a better ML model result. We test clusters  
 130 based on  $K = 2$ ,  $K = 4$ , and  $K = 8$ , which each produce climatologically coherent  
 131 station groups. The result for  $K = 2$  divides stations into two main groups correspond-  
 132 ing to northern and southern China (Fig. 1b), while that for  $K = 4$  produces clusters  
 133 corresponding to the Northeast, North, and South regions along with some scattered sta-  
 134 tions (Fig. 1c). The scattered stations in cluster 3 are grouped because they experience  
 135 much larger wind speeds than their geographic neighbors. The result for  $K = 8$  fur-  
 136 ther distinguishes some sub-regions with distinct climatological characteristics, such as  
 137 the northwestern region and Yunnan Province (Fig. 1d).

### 138 3.2 Temperature post-processing based on LightGBM

139 After clustering, we apply a decision-tree model (Quinlan, 1986) to characterize re-  
 140 lationships between the NWP forecasts and observations, correct biases, and identify how  
 141 different features affect the prediction results. Decision trees are tree-like graph mod-  
 142 els. Information is passed from the root (representing the raw data) and split into branches  
 143 at each level. The splitting rule is typically set by the variable that best discriminates  
 144 among the samples along each branch. Decision trees produce naturally explainable out-  
 145 puts and can provide valuable insight into hidden relationships uncovered by the algo-  
 146 rithm. This method has been successfully employed in a wide variety of weather appli-  
 147 cations (McGovern et al., 2017).

148 Gradient Boosting Decision Tree (GBDT; e.g., Chen & Guestrin, 2016) is a pop-  
 149 ular decision tree approach that involves an ensemble of sequentially-trained decision trees  
 150 and gains knowledge by fitting negative gradients. In this work we use LightGBM (Ke  
 151 et al., 2017), a highly efficient and scalable GBDT algorithm, to explore the relationships  
 152 between NWP forecasts and observations in each cluster. LightGBM has been applied  
 153 to sorting, classification, and regression tasks in a number of big-data studies (e.g., Cao  
 154 & Gui, 2019; Ju et al., 2019). Adopting a leaf-wise growth strategy with depth limita-  
 155 tion and gradient-based one-side sampling, LightGBM seldom overfits on small train-  
 156 ing datasets (Ke et al., 2017). More details on the LightGBM model and its implemen-  
 157 tation in this study are provided in Text S2 and Fig. S2 of the supporting information.

### 158 3.3 Transfer Learning for Newly-built Stations

159 In practice, ML models may malfunction due to data deficiencies or over-fitting.  
 160 Transfer learning helps to reduce the likelihood of these types of failures by transferring  
 161 knowledge from a previously trained model. The transferred model is then fine-tuned  
 162 using newly-added data. This approach has been widely applied, including for the pre-

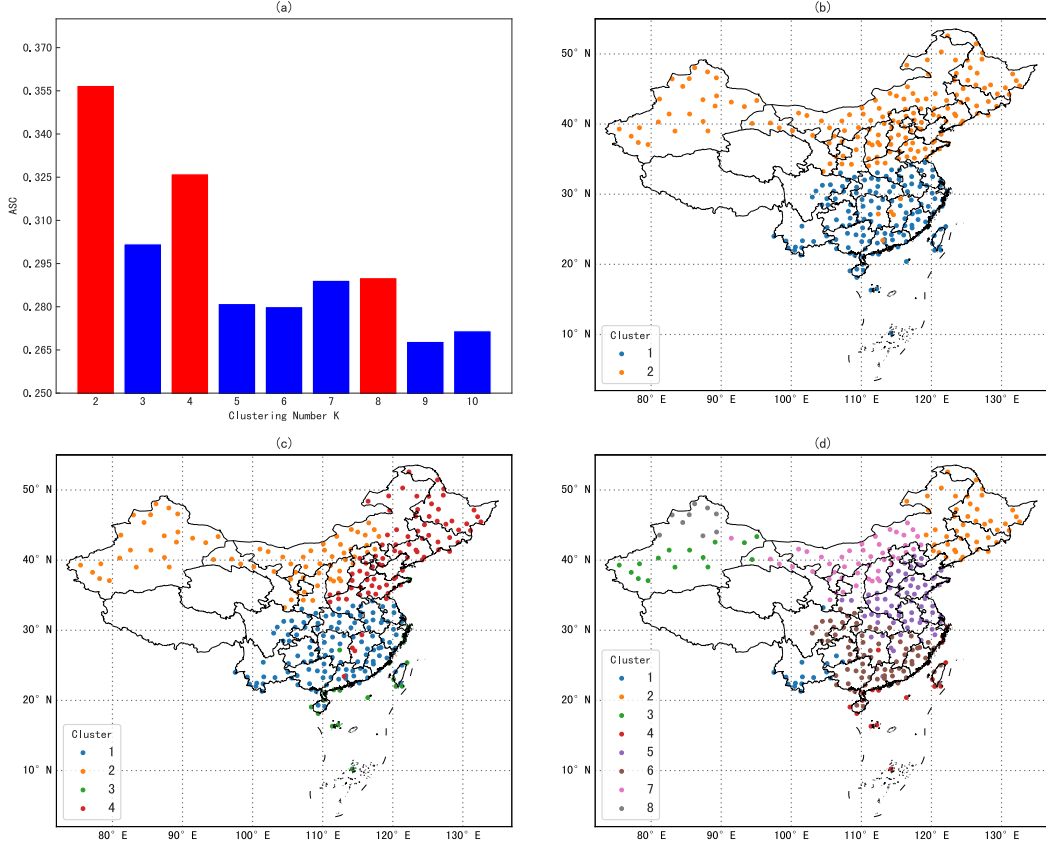


**Figure 1.** The effect of the number of clusters ( $K$ ) on the clustering results. (a) The average Silhouette Coefficient (ASC, Text S1 in SI) as a function of  $K$ . Local maxima occur at  $K = 2$ ,  $K = 4$ , and  $K = 8$ . (b) The spatial distribution of clusters for  $K = 2$ . (c) Same as (b) but for  $K = 4$ . (d) Same as (b) but for  $K = 8$ .

163 diction of wind speed (e.g., Hu et al., 2016; Qureshi & Khan, 2019). The LightGBM model  
 164 for each cluster is taken as a pre-trained model, transferred and further trained on ob-  
 165 servations from newly-built stations identified as belonging to that cluster. The cluster  
 166 to which each new station belongs is determined by static geolocation information along  
 167 with the estimated annual means and standard deviations of key meteorological features  
 168 (surface air temperature, pressure, wind speed, and relative humidity). The latter are  
 169 IDW-interpolated from gridded NWP forecasts to accommodate the limited observational  
 170 records at these stations. The refined LightGBM model is then applied to surface air tem-  
 171 perature forecasts at the newly-built station.

## 172 4 Results

173 Data spanning the six-year period from 2013 to 2018 are divided into three parts.  
 174 Data from 2013 to 2017 are used for training (80% of the data) and validation (the re-  
 175 maining 20%). All data for 2018 are used for testing. We construct a separate model to  
 176 post-process ECMWF forecasts at each lead time (28 in all; Sect. 2) in each cluster. The  
 177 benefits are most significant at short lead times, with error reductions as large as 39.4%  
 178 (1.02°C) for 1-day forecasts (6~24 h lead times; Table 1). Improvements decrease steadily  
 179 to 20.0% (0.68°C) for 7-day forecasts (144~168 h lead times). The average RMSE across  
 180 all lead times is reduced by 0.81°C, corresponding to a 27.9% increase in accuracy. Clus-

181 tering improves the effectiveness of the decision tree algorithm, with the greatest error  
 182 reduction achieved when stations are grouped into four clusters. Compared to models  
 183 without clustering (i.e., a single model trained on all stations), the RMSE is reduced by  
 184 0.54% when two clusters are used ( $K = 2$ ), 0.62% when  $K = 4$ , and 0.41% when  $K =$   
 185 8. Since the  $K = 4$  result produces the smallest RMSE, we adopt this model for all sub-  
 186 sequent experiments. In addition to improving the overall forecast quality, clustering re-  
 187 duces the RMSE at 296 out of 301 individual stations (98.3%) when  $K = 4$  (Fig. 2a).

188 Table 1 and Fig. 2 also show results for three alternative ML algorithms that are  
 189 also widely used in meteorological applications (e.g., Gensler et al., 2017; Akram & El,  
 190 2016; Qing & Niu, 2018; Cao & Gui, 2019): linear regression (LR), artificial neural net-  
 191 work (ANN), and long short-term memory (LSTM) with a fully-connected network (FCN).  
 192 LR, ANN, and LSTM-FCN are used as control models to predict temperature using iden-  
 193 tical inputs. Detailed descriptions of the ANN and LSTM-FCN models are given in Text S3  
 194 and Figs. S3–S4 in the supporting information. The overall RMSE is reduced by 0.49°C  
 195 (16.8%) under LR, 0.71°C (24.7%) under ANN, and 0.71°C (24.7%) under LSTM-FCN  
 196 in the  $K = 4$  scenario, including RMSE reductions at 211 stations under LR (Fig. 2b),  
 197 270 stations under ANN (Fig. 2c), and 272 stations under LSTM-FCN (Fig. 2d). Light-  
 198 GBM outperforms all three models, providing a further reduction of the RMSE for sur-  
 199 face air temperature forecasts of 14.2% relative to LR, 3.8% relative to ANN, and 2.6%  
 200 relative to LSTM-FCN, indicating that LightGBM is more effective for this application.  
 201 LightGBM also takes less time for training ( $\sim 10$  minutes) than ANN ( $\sim 20$  minutes) or  
 202 LSTM-FCN ( $\sim 40$  minutes).

**Table 1.** RMSE of surface air temperature based on five different models for seven different lead times (Unit: °C). See text for details and definitions.

Lead Time	ECMWF	LightGBM	LR	ANN	LSTM-FCN
6~24 h	2.59	<b>1.57</b>	1.94	1.63	1.60
30~48 h	2.72	<b>1.83</b>	2.22	1.91	1.89
54~72 h	2.83	<b>2.00</b>	2.37	2.10	2.09
78~96 h	2.93	<b>2.15</b>	2.48	2.25	2.23
102~120 h	3.05	<b>2.30</b>	2.60	2.40	2.39
126~144 h	3.21	<b>2.49</b>	2.76	2.61	2.61
150~168 h	3.41	<b>2.73</b>	2.95	2.85	2.95

203 Based on these findings, we conclude that LightGBM in combination with four clusters  
 204 presents a substantial improvement over both the original operational forecasts and  
 205 other ML-learning post-processing products. We therefore apply transfer learning to fine-  
 206 tune the LightGBM model for extension to data-poor stations. To replicate the oper-  
 207 ational scenario, we randomly select 20% of the stations to serve as synthetic newly-built  
 208 stations, using the remaining 80% stations to produce pre-trained models for each of the  
 209 four clusters. We then fine-tune the pre-trained models using data covering between zero  
 210 and 24 months at 2-month increments. The use of zero months of data corresponds to  
 211 applying the pre-trained model directly without fine-tuning. We then evaluate the cor-  
 212 rected forecasts for the ‘new’ stations using testing data from the year 2018. To validate  
 213 the transfer learning results, we select seven lead times ranging from 24 h to 168 h at 24-  
 214 h increments. The pre-trained models outperform the original NWP by 0.56°C (16.8%)  
 215 even without fine-tuning (Fig. 3). The RMSE reduction continues to improve as the data  
 216 span used for fine-tuning is extended, reaching 36.4% (1.23°C) when 12 months of data  
 217 are used. Further improvements are negligible, indicating that the fine-tuning benefits  
 218 plateau once the annual cycle is fully represented.

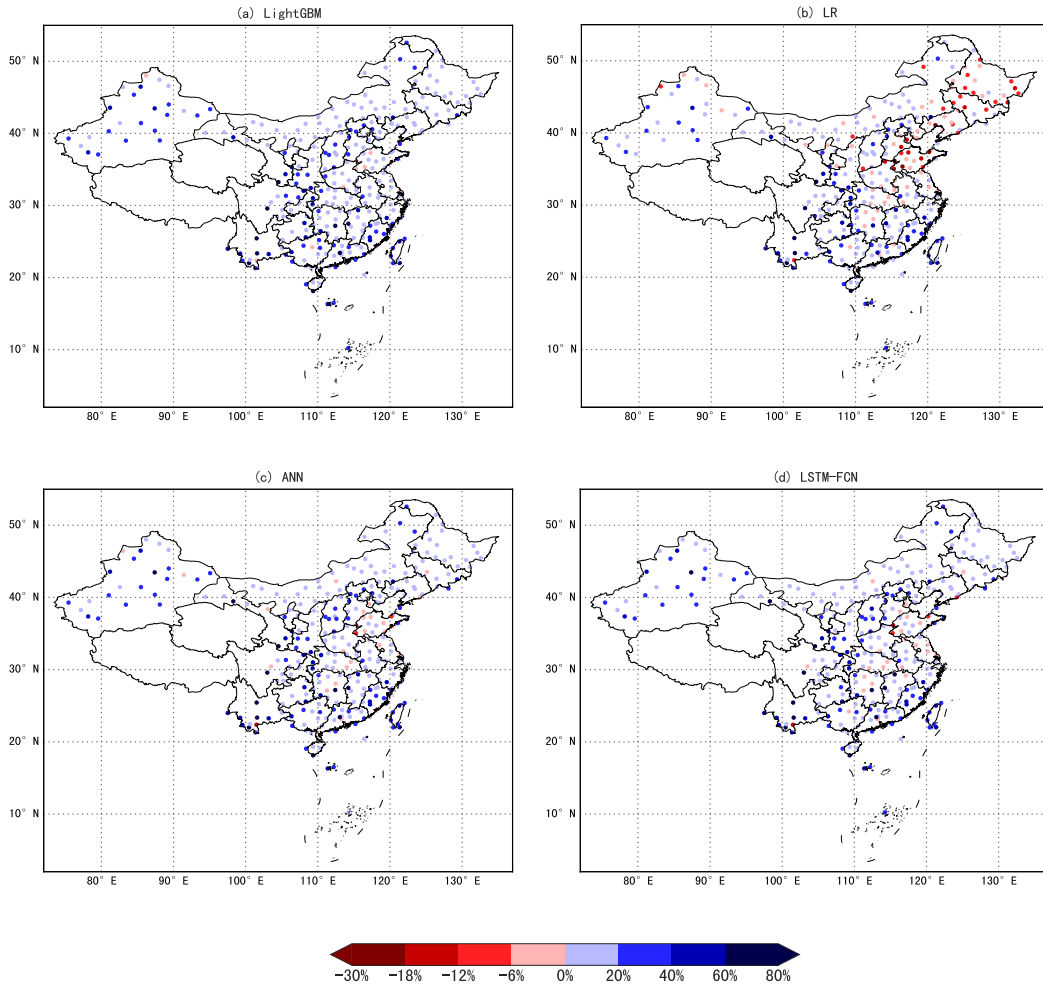


**Figure 2.** Model assessment for test data. (a) Spatial distribution of relative error reduction by the LightGBM model with four clusters. Blue colors indicate improvement; red colors indicate deterioration. (b) Same as (a) but for LR. (c) Same as (a) but for ANN. (d) Same as (a) but for LSTM-FCN.

219 LightGBM, as a GBDT variant, is a ‘grey box’ AI algorithm. Information gain, split  
 220 times, and coverage rate can be calculated for each feature and used to explain the re-  
 221 sults (Gilpin et al., 2019). For example, the raw (NWP) surface air temperature fore-  
 222 cast contributes the most information for most lead times and cluster members when  $K =$   
 223 4 (Fig. 4). Temperature observations are the second most influential feature, but make  
 224 only marginal contributions in most cases. For clusters where the RMSE of the opera-  
 225 tional ECMWF forecasts is already relatively small, such as cluster 2, the NWP fore-  
 226 casts account for a larger proportion of the overall influence. Conversely, observed tem-  
 227 peratures play a larger role for clusters with larger RMSEs in the operational forecasts,  
 228 such as cluster 4. The importance of the operational forecasts also increases as lead time  
 229 increases, with concomitant reductions in the importance of the direct observations.

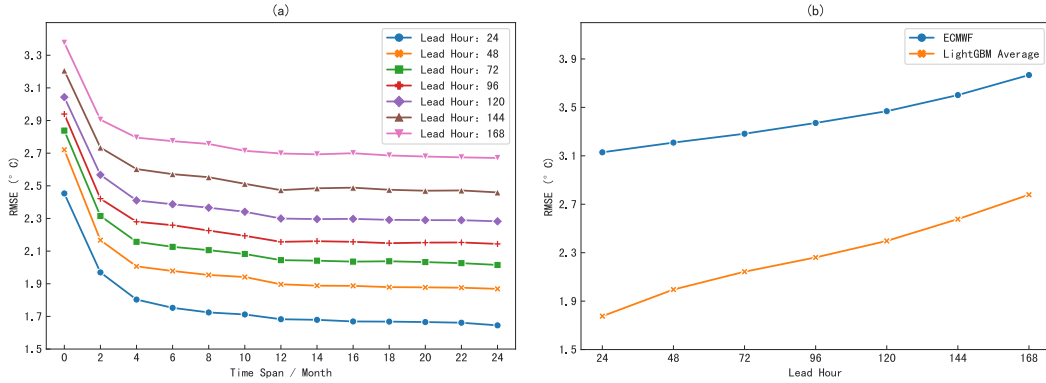


**Figure 3.** Results of transfer learning for the 60 sites randomly selected to serve as synthetic newly-built stations. The time span of training data used to fine-tune the model ranges from zero to 24 months, where zero months means the pre-trained model is used directly without fine-tuning. (a) RMSE values at seven different lead times using pre-trained models based on four clusters. (b) RMSE of the ECMWF forecasts and LightGBM post-processed results at seven different lead times. The LightGBM results reflect average RMSEs for training data time spans ranging from zero to 24 months.

230

## 5 Conclusion

231

232

233

234

235

236

237

238

239

240

241

242

243

244

245

246

247

ML algorithms show great potential for post-processing numerical weather forecasts, but their application is often restricted by the amount of available observations. In this paper we propose the CDT framework, based on clustering, decision tree, and transfer learning, and assess its performance in post-processing ECMWF forecasts of surface air temperature at lead times ranging from 6 to 168 h for 301 weather stations in China. The stations are first divided into two, four, and eight clusters, as these classifications produce climatologically and geographically meaningful station groupings. The CDT framework reduces the average RMSE of temperature forecasts at the 301 stations by up to  $0.81^{\circ}\text{C}$  (27.9%). These benefits are seen for all clustering scenarios and at all lead times, but the greatest improvements are for the 4-cluster scenario at 6–24 h lead times. Transfer learning aids the extension of models trained on data-rich stations to data-sparse stations within the same cluster. The RMSE at new stations is reduced by 16.8% ( $0.56^{\circ}\text{C}$ ) relative to the raw ECMWF forecasts even without fine-tuning, rising to 36.4% ( $1.23^{\circ}\text{C}$ ) once one year of observations is available for fine-tuning the algorithm. These improvements illustrate the great potential of the CDT framework for operational model post-processing, since newly-built sites typically suffer from short data records that restrict the application of AI techniques.

248

249

250

251

252

253

254

An attractive feature of decision tree-based models is that the results can be explained in terms of the contributions from each input feature. Here the main contribution is from the raw ECMWF forecast, especially at longer lead times. However, the station temperature observations are most important contributor for short lead times at stations in cluster 4, where the operational forecasts are less accurate than in other clusters. Overall, the CDT framework can help to correct prediction biases between NWP and observations, especially for newly-built stations or sites with sparse data records.

255

## Acknowledgments

256

257

This work is based on data provided by the TIGGE project and [Meteomanz.com](http://meteomanz.com). TIGGE (The Interactive Grand Global Ensemble) is an initiative of the World Weather Research

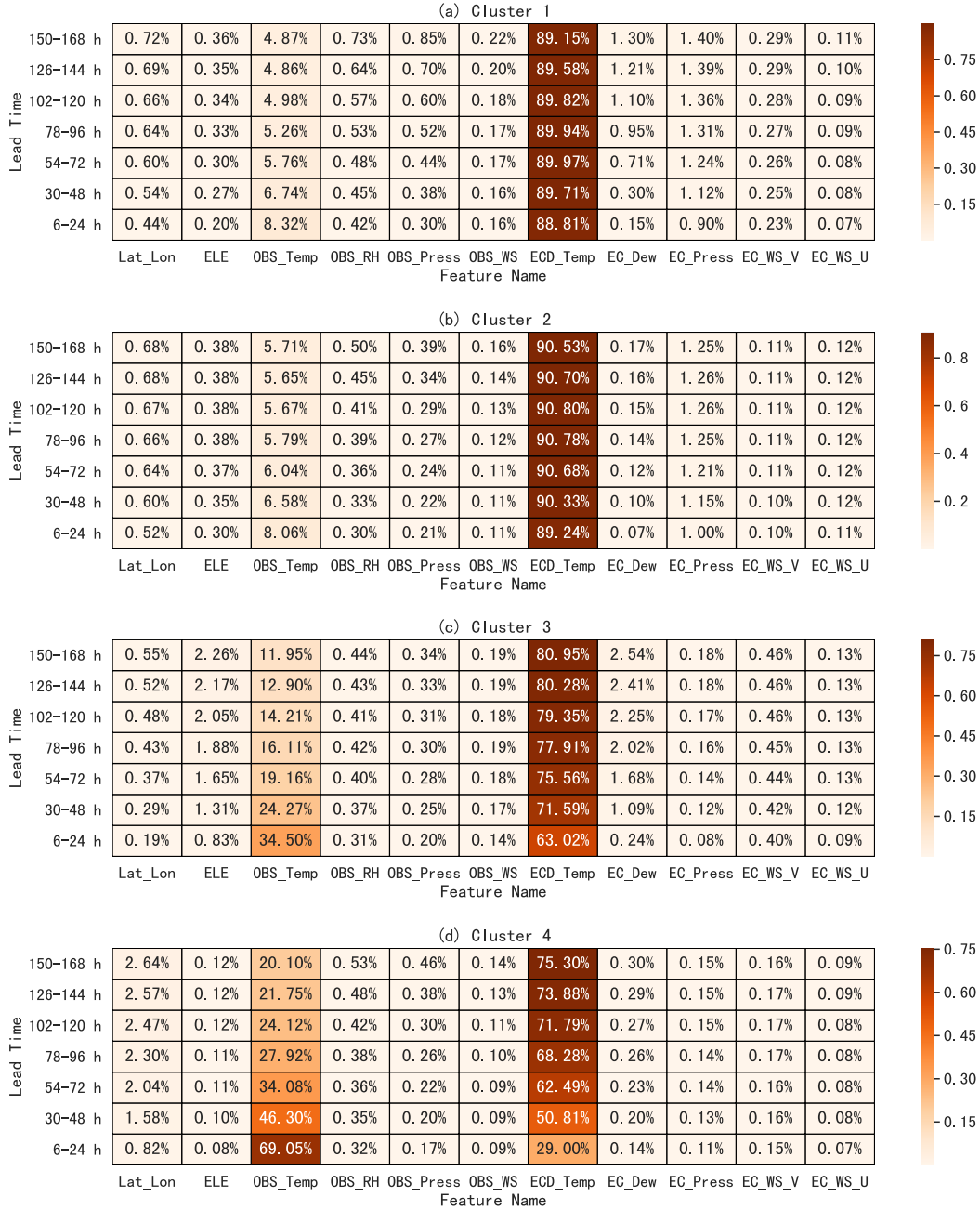


**Figure 4.** The relative importance of features at different lead times and for different clusters. The “EC” prefix indicates variables from the original ECMWF forecasts, while the “OBS” prefix indicates direct observations. Temp stands for temperature; RH for relative humidity; Press for surface pressure; WS for wind speed; dew for dew point temperature; WS\_U and WS\_V for the zonal and meridional components of wind speed, respectively; Lat\_Lon for the latitude and longitude of the station; and ELE for the elevation of the station. The cluster numbers correspond to the  $K = 4$  clustering result (Fig. 1c).

258 Programme (WWRP). [Meteomanz.com](http://meteomanz.com) collects observations released by official weather  
 259 stations. The authors are sponsored by grants from the State's Key Project of Research  
 260 and Development Plan (2016YFB0201100, 2017YFC1502200, 2018YFB0505000, 2018YFB1502800),  
 261 the National Natural Science Foundation of China (41776010), and the Pilot National  
 262 Laboratory for Marine Science and Technology (Qingdao)(QNL2016ORP0108).

## 263 References

- 264 Agapiou, A. (2017). Remote sensing heritage in a petabyte-scale: satellite data and  
 265 heritage Earth Engine© applications. *International Journal of Digital Earth*,  
 266 *10*(1), 85–102. doi: 10.1080/17538947.2016.1250829
- 267 Akram, M., & El, C. (2016). Sequence to Sequence Weather Forecasting with Long  
 268 Short-Term Memory Recurrent Neural Networks. *International Journal of*  
 269 *Computer Applications*, *143*(11), 7–11. doi: 10.5120/ijca2016910497
- 270 Bador, M., Naveau, P., Gilleland, E., Castellà, M., & Arivelo, T. (2015). Spatial  
 271 clustering of summer temperature maxima from the CNRM-CM5 climate  
 272 model ensembles & E-OBS over Europe. *Weather and Climate Extremes*, *9*,  
 273 17–24. doi: 10.1016/j.wace.2015.05.003
- 274 Bauer, P., Thorpe, A., & Brunet, G. (2015). The quiet revolution of numerical  
 275 weather prediction. *Nature*, *525*(7567), 47–55. doi: 10.1038/nature14956
- 276 Bernard, E., Naveau, P., Vrac, M., & Mestre, O. (2013). Clustering of maxima: Spa-  
 277 tial dependencies among heavy rainfall in france. *Journal of Climate*, *26*(20),  
 278 7929–7937. doi: 10.1175/JCLI-D-12-00836.1
- 279 Boers, N., Goswami, B., Rheinwalt, A., Bookhagen, B., Hoskins, B., & Kurths, J.  
 280 (2019). Complex networks reveal global pattern of extreme-rainfall teleconnec-  
 281 tions. *Nature*, *566*(7744), 373–377. doi: 10.1038/s41586-018-0872-x
- 282 Bougeault, P., Toth, Z., Bishop, C., Brown, B., Burridge, D., De Chen, H., ...  
 283 Worley, S. (2010). The thorpex interactive grand global ensemble. *Bul-*  
 284 *letin of the American Meteorological Society*, *91*(8), 1059–1072. doi:  
 285 10.1175/2010BAMS2853.1
- 286 Cao, Y., & Gui, L. (2019). Multi-Step wind power forecasting model Using LSTM  
 287 networks, Similar Time Series and LightGBM. *2018 5th International Confer-*  
 288 *ence on Systems and Informatics, ICSAI 2018*(Icsai), 192–197. doi: 10.1109/  
 289 ICSAI.2018.8599498
- 290 Chen, T., & Guestrin, C. (2016, 3). XGBoost: A scalable tree boosting system. *Pro-*  
 291 *ceedings of the ACM SIGKDD International Conference on Knowledge Discov-*  
 292 *ery and Data Mining, 13-17-Augu*, 785–794. doi: 10.1145/2939672.2939785
- 293 Gensler, A., Henze, J., Sick, B., & Raabe, N. (2017). Deep Learning for so-  
 294 lar power forecasting - An approach using AutoEncoder and LSTM Neu-  
 295 ral Networks. *2016 IEEE International Conference on Systems, Man, and*  
 296 *Cybernetics, SMC 2016 - Conference Proceedings*(April), 2858–2865. doi:  
 297 10.1109/SMC.2016.7844673
- 298 Gentine, P., Pritchard, M., Rasp, S., Reinaudi, G., & Yacalis, G. (2018). Could Ma-  
 299 chine Learning Break the Convection Parameterization Deadlock? *Geophysical*  
 300 *Research Letters*, *45*(11), 5742–5751. doi: 10.1029/2018GL078202
- 301 Gilpin, L. H., Bau, D., Yuan, B. Z., Bajwa, A., Specter, M., & Kagal, L. (2019).  
 302 Explaining explanations: An overview of interpretability of machine learning.  
 303 *Proceedings - 2018 IEEE 5th International Conference on Data Science and*  
 304 *Advanced Analytics, DSAA 2018*, 80–89. doi: 10.1109/DSAA.2018.00018
- 305 Glahn, H. R., & Lowry, D. A. (1972). *The Use of Model Output Statistics (MOS) in*  
 306 *Objective Weather Forecasting* (Vol. 11) (No. 8). doi: 10.1175/1520-0450(1972)  
 307 011(1203:tuomos)2.0.co;2
- 308 Ham, Y.-g., Kim, J.-h., & Luo, J.-j. (2019, 9). Deep learning for multi-year ENSO  
 309 forecasts. *Nature*. doi: 10.1038/s41586-019-1559-7
- 310 Hastie, T., Tibshirani, R., & Friedman, J. (2009). *The Elements of Statistical Learn-*

- 311        *ing* (Vol. 27) (No. 2). New York, NY: Springer New York. doi: 10.1007/978-0  
312        -387-84858-7
- 313        Hu, Q., Zhang, R., & Zhou, Y. (2016). Transfer learning for short-term wind speed  
314        prediction with deep neural networks. *Renewable Energy*, 85, 83–95. doi: 10  
315        .1016/j.renene.2015.06.034
- 316        Hwang, J., Orenstein, P., Cohen, J., Pfeiffer, K., & Mackey, L. (2019). Improving  
317        subseasonal forecasting in the western U.S. With machine learning. *Proceedings*  
318        *of the ACM SIGKDD International Conference on Knowledge Discovery and*  
319        *Data Mining*, 2325–2335. doi: 10.1145/3292500.3330674
- 320        Jiang, G. Q., Xu, J., & Wei, J. (2018). A Deep Learning Algorithm of Neural  
321        Network for the Parameterization of Typhoon-Ocean Feedback in Typhoon  
322        Forecast Models. *Geophysical Research Letters*, 45(8), 3706–3716. doi:  
323        10.1002/2018GL077004
- 324        Ju, Y., Sun, G., Chen, Q., Zhang, M., Zhu, H., & Rehman, M. U. (2019). A model  
325        combining convolutional neural network and lightgbm algorithm for ultra-  
326        short-term wind power forecasting. *IEEE Access*, 7(c), 28309–28318. doi:  
327        10.1109/ACCESS.2019.2901920
- 328        Ke, G., Meng, Q., Finley, T., Wang, T., Chen, W., Ma, W., . . . Liu, T. Y. (2017).  
329        LightGBM: A highly efficient gradient boosting decision tree. *Advances in*  
330        *Neural Information Processing Systems, 2017-Decem(Nips)*, 3147–3155.
- 331        Lynch, P. (2008). The origins of computer weather prediction and climate modeling.  
332        *Journal of Computational Physics*, 227(7), 3431–3444. doi: 10.1016/j.jcp.2007  
333        .02.034
- 334        McGovern, A., Elmore, K. L., Gagne, D. J., Haupt, S. E., Karstens, C. D.,  
335        Lagerquist, R., . . . Williams, J. K. (2017). Using artificial intelligence  
336        to improve real-time decision-making for high-impact weather. *Bul-*  
337        *letin of the American Meteorological Society*, 98(10), 2073–2090. doi:  
338        10.1175/BAMS-D-16-0123.1
- 339        Myers, D. E. (1994). Spatial interpolation: an overview. *Geoderma*, 62(1-3), 17–28.  
340        doi: 10.1016/0016-7061(94)90025-6
- 341        Overpeck, J. T., Meehl, G. A., Bony, S., & Easterling, D. R. (2011, 2). Climate Data  
342        Challenges in the 21st Century. *Science*, 331(6018), 700–702. doi: 10.1126/  
343        science.1197869
- 344        Pan, B., Hsu, K., AghaKouchak, A., & Sorooshian, S. (2019). Improving Precipi-  
345        tation Estimation Using Convolutional Neural Network. *Water Resources Re-*  
346        *search*, 55(3), 2301–2321. doi: 10.1029/2018WR024090
- 347        Pan, S. J., & Yang, Q. (2010, 10). A Survey on Transfer Learning. *IEEE Trans-*  
348        *actions on Knowledge and Data Engineering*, 22(10), 1345–1359. doi: 10.1109/  
349        TKDE.2009.191
- 350        Qing, X., & Niu, Y. (2018). Hourly day-ahead solar irradiance prediction using  
351        weather forecasts by LSTM. *Energy*, 148, 461–468. doi: 10.1016/j.energy.2018  
352        .01.177
- 353        Quinlan, J. R. (1986, 3). Induction of decision trees. *Machine Learning*, 1(1), 81–  
354        106. doi: 10.1007/BF00116251
- 355        Qureshi, A. S., & Khan, A. (2019). Adaptive transfer learning in deep neural net-  
356        works: Wind power prediction using knowledge transfer from region to region  
357        and between different task domains. *Computational Intelligence*, 35(4), 1089–  
358        1113. doi: 10.1111/coin.12236
- 359        Rasp, S., & Lerch, S. (2018, 11). Neural Networks for Postprocessing Ensemble  
360        Weather Forecasts. *Monthly Weather Review*, 146(11), 3885–3900. doi: 10  
361        .1175/MWR-D-18-0187.1
- 362        Rasp, S., Pritchard, M. S., & Gentine, P. (2018, 9). Deep learning to represent sub-  
363        grid processes in climate models. *Proceedings of the National Academy of Sci-*  
364        *ences*, 115(39), 9684–9689. doi: 10.1073/pnas.1810286115
- 365        Reichstein, M., Camps-Valls, G., Stevens, B., Jung, M., Denzler, J., Carvalhais,

- 366 N., & Prabhat. (2019, 2). Deep learning and process understanding  
367 for data-driven Earth system science. *Nature*, *566*(7743), 195–204. doi:  
368 10.1038/s41586-019-0912-1
- 369 Rousseeuw, P. J. (1987). Silhouettes: A graphical aid to the interpretation and vali-  
370 dation of cluster analysis. *Journal of Computational and Applied Mathematics*,  
371 *20*(C), 53–65. doi: 10.1016/0377-0427(87)90125-7
- 372 Runge, J., Bathiany, S., Camps-Valls, G., Coumou, D., Deyle, E., Kretschmer,  
373 M., . . . Zscheischler, J. (2019). Inferring causation from time series  
374 in Earth system sciences. *Nature Communications*, *10*(1), 2553. doi:  
375 10.1038/s41467-019-10105-3
- 376 Scher, S. (2018). Toward Data-Driven Weather and Climate Forecasting: Approxi-  
377 mating a Simple General Circulation Model With Deep Learning. *Geophysical*  
378 *Research Letters*, *45*(22), 616–12. doi: 10.1029/2018GL080704
- 379 Schneider, T., Lan, S., Stuart, A., & Teixeira, J. (2017). Earth System Modeling 2.0:  
380 A Blueprint for Models That Learn From Observations and Targeted High-  
381 Resolution Simulations. *Geophysical Research Letters*, *44*(24), 396–12. doi:  
382 10.1002/2017GL076101
- 383 Shi, X., Chen, Z., & Wang, H. (2015). Convolutional LSTM Network: A Machine  
384 Learning Approach for Precipitation Nowcasting. *Nips*, 2–3. doi: 10.1007/978  
385 -3-319-21233-3\_6
- 386 Swinbank, R., Kyouda, M., Buchanan, P., Froude, L., Hamill, T. M., Hewson,  
387 T. D., . . . Yamaguchi, M. (2016). The TIGGE project and its achieve-  
388 ments. *Bulletin of the American Meteorological Society*, *97*(1), 49–67. doi:  
389 10.1175/BAMS-D-13-00191.1